UNIVERSITY OF MISKOLC
FACULTY OF MECHANICAL ENGINEERING AND INFORMATICS

HARVESTING ENERGY FOR ERS AUTOMOBILITY

Booklet of PhD Theses

PREPARED BY:
MOHAMMED ALAA ALWAFAIE

ISTVÁN SÁLYI DOCTORAL SCHOOL OF MECHANICAL ENGINEERING SCIENCES
TOPIC FIELD OF BASIC ENGINEERING SCIENCES
TOPIC GROUP OF MECHANICS OF SOLIDS

Head of Doctoral School
Dr. Gabriella Vadászné Bognár
DSc, Full Professor

Head of Topic Group
Dr. György Szeidl
Full Professor

Scientific Supervisor
Dr. Béla Kovács

Miskolc
2025

JUDGING COMMITTEE

chair

secretary

members

OFFICIAL REVIEWERS

1. INTRODUCTION, THE AIM OF THE RESEARCH WORK

1.1 INTRODUCTION

Energy Recovery Systems (ERS) have emerged as a pivotal solution for enhancing energy efficiency, mitigating environmental degradation, and supporting global sustainability objectives particularly within the automotive industry[1][2].These systems are engineered to reclaim energy that would otherwise be lost during standard vehicle operation and convert it into a usable form that can be stored and redeployed. Modern ERS technologies can capture various forms of energy, including kinetic, thermal, and multi-modal energy, from mechanical and electrical subsystems. This recovered energy is then reintegrated into the vehicle's propulsion system or auxiliary components. The primary objectives of ERS are to optimize energy utilization, minimize waste, and reduce the carbon footprint associated with conventional combustion-based propulsion systems[3].To achieve these objectives, ERS operate through a comprehensive framework consisting of four fundamental stages[4]: energy capture, energy conversion, energy storage ,and energy reuse [5][6][7][8].This integrated architecture enhances both vehicle performance and operational efficiency by supplementing or, in certain applications, replacing traditional energy inputs. Following the energy capture phase, the system proceeds to the conversion stage, where energy is transformed into a usable electrical format. This conversion is typically performed by motor-generator units (MGUs), which convert mechanical motion into electrical power. The Motor Generator Unit-Kinetic (MGU-K) exemplifies this process; it operates during vehicle deceleration capturing kinetic energy from braking and converting it into electrical energy that can be stored and later utilized during acceleration. This capability significantly enhances the energy efficiency and driving range of hybrid and electric vehicles. Complementing MGU-K is the Motor Generator Unit-Heat (MGU-H), which targets thermal energy lost through exhaust gases. The MGU-H incorporates a turbine to extract heat from the exhaust stream and convert it into rotational motion, which in turn drives an electrical generator [9].The resulting electricity may be stored or directly used to power the turbocharger, thereby reducing turbo lag and improving throttle responsiveness. The operation of MGU-H is governed by electromagnetic principles, particularly Lorentz and Laplace force laws, which describe the interaction between magnetic fields and electric currents during energy conversion. Once the energy is converted, it is transferred to the energy storage subsystem. Storage solutions include high-efficiency devices such as lithium-ion batteries [10], supercapacitors [11], and mechanical flywheels [12], all of which retain the recovered energy until it is required. The capacity, responsiveness, and durability of these storage systems directly influence the effectiveness of the ERS, making them essential to overall system performance[13]. Reliable energy storage ensures the immediate availability of power during high demand driving conditions or sudden acceleration events.

The final stage of the ERS cycle is energy reuse. In this phase, stored energy is either redirected to support auxiliary systems or reintroduced into the drivetrain. Control Electronics (CE) manages the flow of power between MGU-K, MGU-H, and the battery. These units are responsible for converting alternating current (AC) from the MGUs into direct current (DC) for storage [14] and, when necessary, reversing the process. The CE employs insulated gate bipolar

transistors (IGBTs) and capacitors to regulate this bidirectional power flow. Low-voltage logic boards control high-voltage circuits, ensuring safe and precise energy distribution. As a result, the ERS can operate without a traditional alternator, while providing a stable 12–24 V supply to onboard auxiliary systems. It is important to note that real-world ERS implementations, particularly those in Formula One, are significantly more sophisticated than the generalized systems described herein[3].They may include additional subsystems and advanced control mechanisms to further enhance efficiency, responsiveness, and integration. These systems not only demonstrate the potential of ERS technology but also offer a promising foundation for future advancements in sustainable automotive engineering.

1.2 THE AIM OF THE RESEARCH WORK

In this comprehensive study, it will be exploring various other types of energy harvesting that can be incorporated into the system to enhance efficiency and foster the development of technical advancements with potential benefits for passenger car applications. So that, I am dedicated to advancing achieving energy efficiency in the automotive industry, particularly for electric vehicles, promote sustainable designs and improve energy utilization.

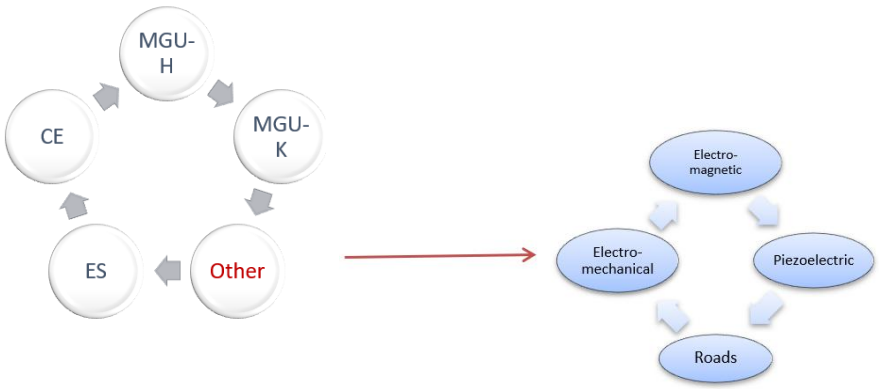

Figure 1.1 The scheme of other harvesting energy

This research explores advanced methodologies as in figure 1.1, for harvesting energy from routine vehicular dynamics such as wheel rotation and road interaction with the aim of enhancing energy efficiency and contributing to the sustainability of the passenger vehicle industry. The study integrates empirical measurements and analytical modeling to evaluate and improve energy recovery strategies.

The central focus of this work is the development and integration of novel energy harvesting technologies that can significantly augment the functional capabilities and economic viability of automotive manufacturing. One promising avenue involves the exploitation of electromagnetic phenomena to generate electricity from vehicular motion. A comprehensive review of existing energy harvesting systems was conducted, including the studies by (Aksu & Halicioglu, 2018)[15] which provide a broad overview of vehicular energy harvesting technologies, and (Sultoni et al., 2013)[16], who investigated vibration energy harvesting using rotary and linear electromagnetic generators. Additionally, the work by Wang et al. (2012)[17], demonstrated the feasibility of wideband electromagnetic energy harvesting from rotating

wheels using a Halbach array magnetic disk, achieving power outputs in the range of 300–550 μW at 200–500 rpm. Building on these foundations, This concept, which I have developed, outlines a method that can assist vehicles in reducing electricity consumption for components such as lamps and air conditioning. Additionally, the concept of Multi-Modal Energy Harvesting involves creating a hybrid system that integrates electromagnetic and various other energy harvesting methods to capture energy from multiple sources within a vehicle. This multi-modal approach has the potential to significantly enhance overall energy efficiency and provide a more reliable energy supply for electric vehicles. Piezoelectric materials, which convert mechanical vibrations into electrical energy, represent another promising technology. These materials can be embedded within vehicle wheels or road surfaces to capture vibrational energy as the recent studies, such as Zhou et al. (2023) [18], have summarized the state of road energy harvesting technology. In my thesis, it introduces a novel methodology that dynamically analyzes vehicle motion data to optimize energy recovery strategies, potentially leading to more intelligent and adaptive energy management systems in electric vehicles. Furthermore, this research explores the role of energy harvesting in the development of "Smart Roads," a critical component of the broader "Smart City" initiative. Studies (Lazaroi et al., 2012)[19], (Wang et al., 2020)[20] , and (Wu et al. 2019)[21] have investigated the integration of piezoelectric energy harvesting (PEH) and triboelectric nanogenerators (TENGs) into road infrastructure. These technologies, enhanced by nanotechnology, enable roads to convert the kinetic energy of passing vehicles into usable electrical energy, thereby reducing dependence on traditional charging infrastructure. Finally,I have discovered a novel approach to generating electricity using a Mechanical Motion Rectifier (MMR), a concept that has yet to be invented by anyone else. This innovative technology harnesses energy when the brake or throttle pedal is engaged in automotive applications. My goal is to explore the impact of vehicle dynamics on energy recovery systems through groundbreaking research. By examining how various vehicle designs and dynamics influence the efficiency of energy recovery, we can develop tailored vehicle designs that optimize energy harvesting for specific driving conditions. Furthermore, integrating AI can enhance the performance of batteries in electric vehicles, making this idea even more promising. By exploring these innovative ideas, my research could contribute to the development of more sustainable and technologically advanced vehicles.

2. METHODOLOGY

2.1 ELECTROMAGNETIC EFFECTS FOR OTHER HARVESTING ENERGY

In the context of this research, electromagnetic induction is adopted as the primary mechanism for energy harvesting, specifically within automotive systems. The study focuses on capturing energy generated by wheel rotation, utilizing electromagnetic effects. Two configurations have been examined: the Radial Design (RD) and the Axial Design (AD). Both designs operate based on the interaction between permanent magnets and conductive coils, through which relative motion induces voltage. The design methodology encompasses theoretical modeling, simulation, and experimental validation of the proposed energy harvesting systems. These configurations are governed by the fundamental principle of Faraday's Law [22]of Electromagnetic Induction, which states that an electromotive force (EMF) is induced in a coil when there is a time-varying magnetic flux through its surface:

$$\varepsilon = \oint (\dot{r} \times B)\, dl \tag{2.1}$$

This principle forms the foundation for the voltage generation mechanism in both RD and AD systems, enabling the conversion of mechanical motion into usable electrical energy. In the RD configuration, permanent magnets are mounted around the periphery of a rotating wheel. Stationary coils are positioned to intercept the magnetic field as the wheel spins.

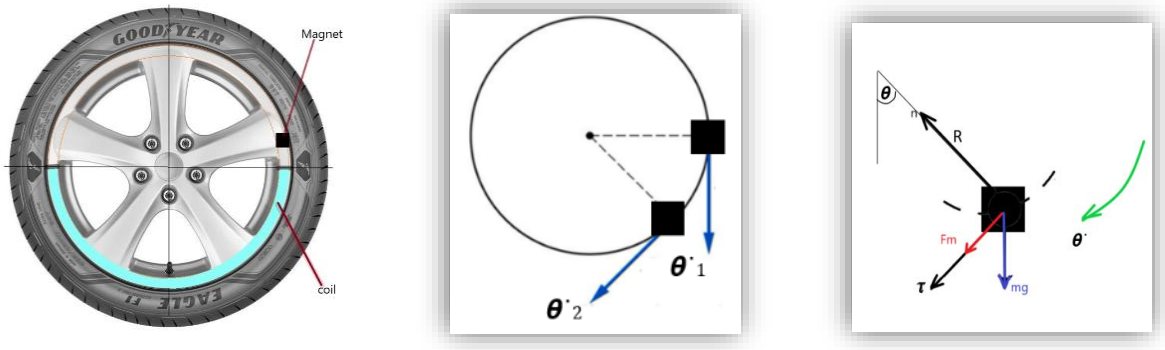

Figure 2.1 The simple drawing about placement of magnetic and coil for RD case

Based on Newton's Second Law of Motion [23], the dynamics of magnetic movement in the context of wheel-based energy harvesting can be described by analyzing the magnetic field at the center of the coil, as well as the motion of the magnet along a partial (half) arc of the wheel. This motion can be characterized in terms of the angular position of the magnet, often referred to as the position of magnetic or swing angle (θ). The resulting equations of motion provide a foundational framework for modeling the interaction between the rotating magnet and the induced electromagnetic response in the coil. The parameter K_v which quantifies acceptable vibration levels in passenger vehicles and the value of typically lies within the range of 0.20 to 0.25 and the electromagnetic constant :

$$K_m = \frac{\mu_\circ\, l}{4\,\pi\, r} \tag{2.1}$$

$$\ddot{\theta} + \frac{K_v}{m}\dot{\theta} - \frac{K_m}{m.r}\theta.I^2 - \frac{g}{r}.\sin\theta = 0 \quad (2.2)$$

$$\ddot{\theta} + K_1\dot{\theta} - K_2\theta.I^2 - K_3\sin\theta = 0 \quad (2.3)$$

Table 2. 1 Measured parameters for simulation radial design

Name	Notation	Value and unit
Mass of magnetic	m	0.01 Kg
Length of coil	l	10 m
Radius of wheel	r	0.1925m
Magnetic permeability	μ_0	$4\pi\cdot10^{-7}$ H/m
Coil inductance	L	10 H
Copper coil Resistance	R_c	0.17 Ω

By MATLAB/Simulink we found :

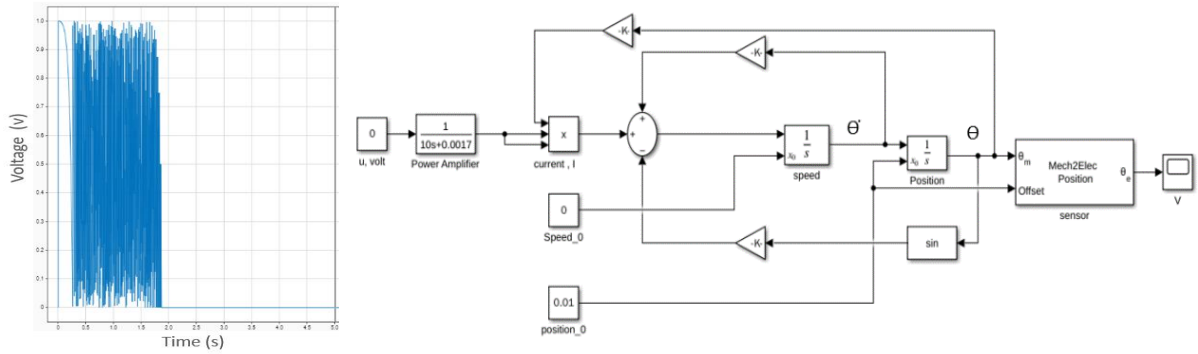

Figure 2.2 The response of system according to time

The response time chart shows that the extracted output voltage is approximately 1.05 volts, which is slightly lower than expected based on this study. This voltage level is sufficient for small applications in automotive systems; however, further investigation is necessary. Therefore, we should explore alternative designs as study in axial design to optimize performance and assess their potential.

In the AD configuration, magnets move axially through stationary coils (e.g., via spokes). The system is analyzed in polar coordinates to capture radial and angular dynamics:

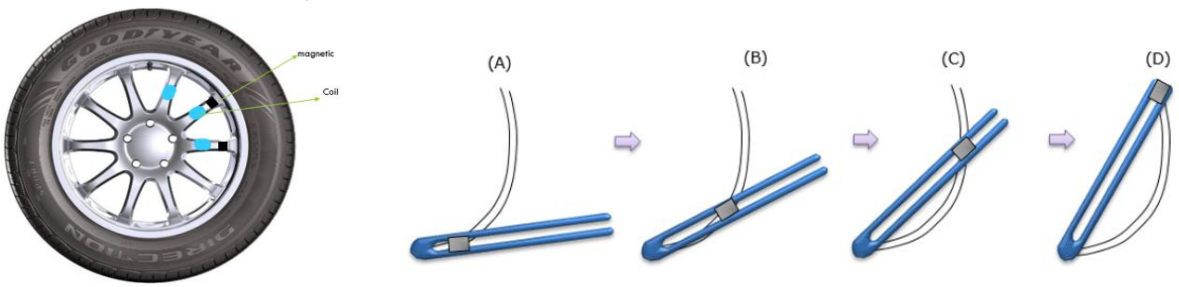

Figure 2.3 The simple drawing about placement of magnetic and coil for AD case

By analyzes the radial and tangential forces acting on a magnet in an energy harvesting system with using Newton's Second Law to model the motion and according to my puplishing[24], it was found that the coupling factor is related by the electromagnetic force to the current flowing

through the coil. he radial velocity $\dot{r}$ represents how quickly the magnet's position changes with respect to the center of rotation. As the magnet moves, it experiences an electromagnetic drag force that opposes its motion. This interaction leads to energy transfer into the electrical circuit.

$$\gamma_r = \frac{F_m}{I}$$

$$F_m = \gamma_r . I \tag{2.4}$$

Following the law of conservation of energy, the power lost by the magnet due to this electromagnetic drag is equal to the power gained by the connected circuit. This process ensures that energy is conserved in the system and confirms that the electromagnetic drag force is directly responsible for converting mechanical motion into electrical energy.

$$\varepsilon . I = \dot{r} . F_m$$

$$\varepsilon . I = \dot{r} . \gamma_r . I$$

$$\gamma_r = \frac{\varepsilon}{\dot{r}} \tag{2.5}$$

As Faraday Law of induction , we can write:

$$\gamma_r = \oint (B_\chi)\, dl \tag{2.6}$$

B= constant for all loops:

$$\gamma_r = \frac{\mu_\circ I R^2 . L}{2 \sqrt[2]{(X^2+R^2)^3}} \tag{2.7}$$

B ≠ constant for loops of coil:

$$\gamma_r = \frac{1}{v} \iiint \left(\frac{\mu_\circ I R^3}{2 \sqrt[2]{(X^2+R^2)^3}} dv\right) . dR . da . d\Theta \tag{2.8}$$

Two experimental setups were tested:

1. <u>Free-Fall Test:</u> A cylindrical magnet was dropped through a coil enclosed in a pipe. The rapid change in magnetic flux induced a voltage spike. The measured energy output was 3.77 mJ

Table 2.2 The specification about disc magnet in free falling test

H (High)	19 mm
D (Diameter)	12.5 mm
m (mass)	18.5 Kg
length of dropping the magnetic	160 mm

Table 2. 3 The specification of the coil in free falling test

H (High)	30.2 mm
R (resistance)	429 Ω
L (inductance)	0.98 H
R_1 (the inner radius of the loop)	13.1 mm
R_2 (the outer radius of the loop)	27.6 mm
a_1 (the beginning radial position of the coil)	58.4 mm
a_2 (the last radial position of the coil)	88.6 mm

Table 2. 4 The specification of the PP pipe in free falling test

Type	Poly Propylene grey RAL 7032 DN 150
Length	153 mm

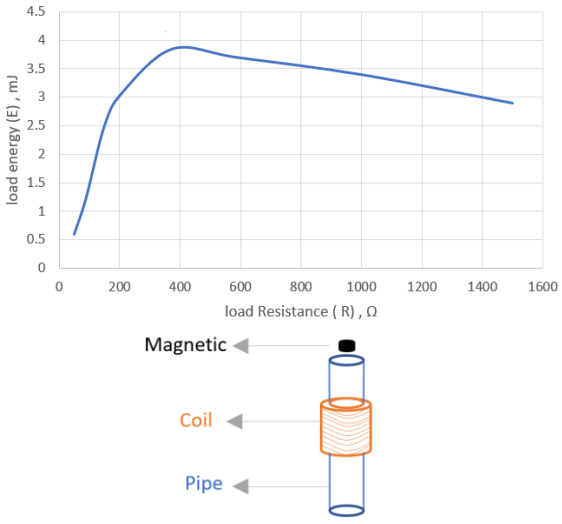

Figure 2.4 The free test information

2. Rotational Wheel Test: Magnets affixed to a rotating wheel generated voltage in stationary coils at varying speeds. Simulation models, developed in MATLAB/Simulink, confirmed experimental results with an error margin of less than 2%.

Table 2. 5 The specification of disc magnet in rotation motion test

H (High)	19 mm
D (Diameter)	12.5 mm
m (mass)	18.5 Kg

Table 2. 6 The specification of the coil in rotation motion test

H (High)	30.2 mm
R (resistance)	429 Ω
L (inductance)	0.98 H
R_1 (the inner radius of the loop)	13.1 mm
R_2 (the outer radius of the loop)	27.6 mm
a_1 (the beginning radial position of the coil)	77.8 mm
a_2 (the last radial position of the coil)	103.0 mm

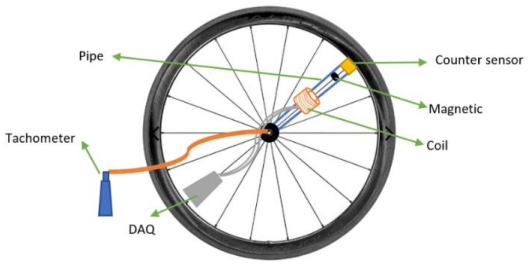

Table 2. 7 The specification of the PP pipe in rotation motion test

Type	Poly Propylene grey RAL 7032 DN 150
Length	153 mm

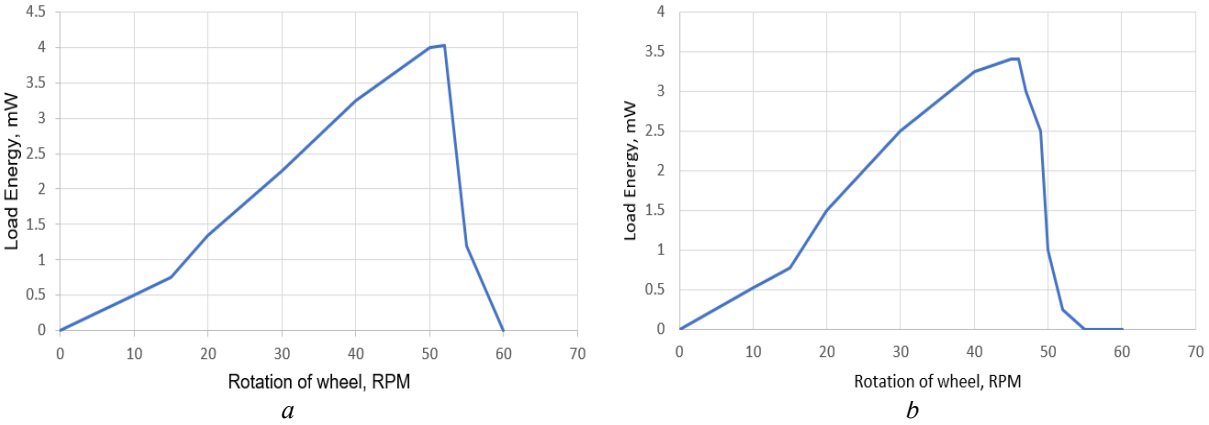

Figure 2.5 The relationship between the energy and rotation of the wheel for (a. without friction, b. with friction)

2.2 PIEZOELECTRIC EFFECTS FOR OTHER HARVESTING ENERGY

Piezoelectric materials are smart materialsthat generate electric charge when subjected to mechanical stress direct piezoelectric effect and deform under electric fields reverse effect [25]. Commonly used materials include Lead Zirconate Titanate (PZT) and $BaTiO_3$, known for their electromechanical coupling efficiency. The material's behavior is governed by constitutive relationships using constants like d_{33} and d_{31} [26] representing polarization along axes as figure 2.6

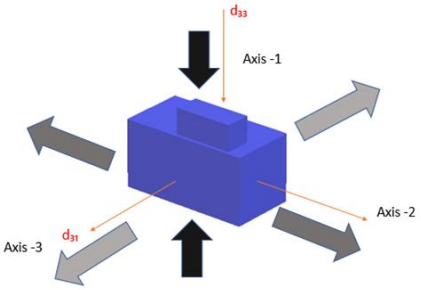

Figure 2. 6 The three-axis direction of the piezoelectric material

Two case studies are presented:

2.2.1 Piezoelectric within the tire (first case)

PZT-5J modules are mounted along the tire's inner circumference to capture mechanical stress from road contact. Generated voltage is stored in a battery. The Characteristic of PZT-5J from PIEZO company and depending on technical data sheet gives in table 2.8:

Table 2. 8 Characteristic of PZT-5J

Piezo electric charge constant	$d_{33} = 48510^{-12}$ C/m²
Piezo voltage coefficient	$g_{33} = 21.3 \times 10^{-3}$ Vm/N
Resonant Thickness	$\tau = 2 \times 10^{-3}$ m
Curie Point	270 °C
Mechanical Quality Factor	60
Frequency Constants Radial	191 kHz · cm
Poisson's Ratio	0.31
Dielectric Constant (1kHz)	KT_3 =2100
Dielectric Loss Factor (1kHz)	0.2%
Clamped Dielectric Constant	800

The total tension will be equal $(\sigma_b + \sigma)$ when there is bending. The value of open circuit voltage will be equal 0.81 volt without bending and 0.92 volt with the bending also the thickness of wheel about 0.05m. The power due to piezoelectric cell compression can determine in equation (2.9), it is the amount of energy that can be obtained from straining or modulating a PZ cell.

$$P = \frac{V_{oc} \times C\prime_d}{\mathrm{t}} \tag{2.9}$$

$C'_d = C_d \times \mathrm{A}$, $C_d = d_{33} \times \sigma_{total}$, $V_{oc} = g_{33} \times \tau \times \sigma$: $\sigma = \frac{\mathrm{F}}{A'}$

The value of power when there is bending for wheel it gives about 0.16 µW for one sec and without bending it about 0.13 µW. The power generated by piezoelectric cells is influenced by stress and the contact area, for known load but when different loads act on the cell, studying the stress and its calculation becomes crucial because increased stress leads to higher open-circuit voltage and charge density.

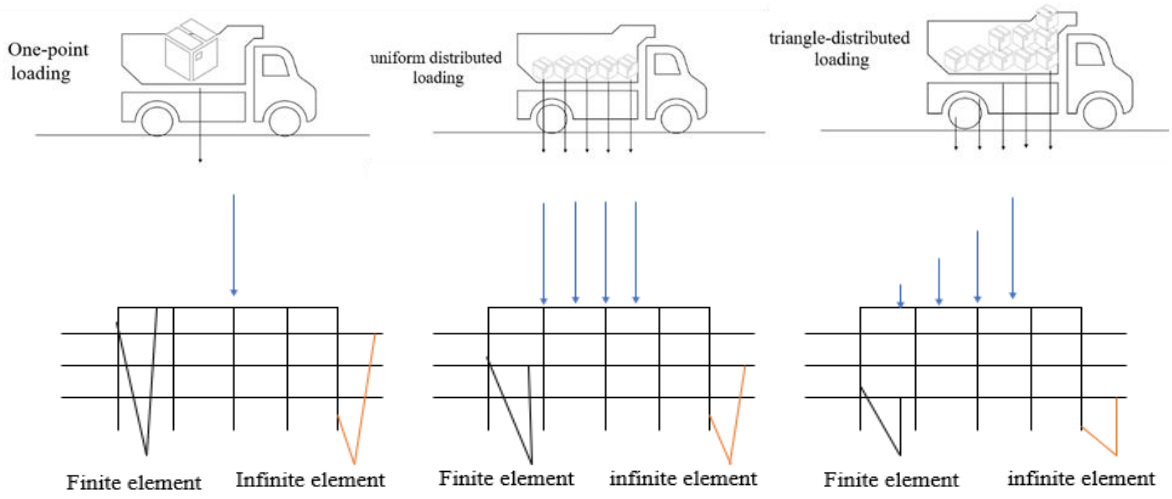

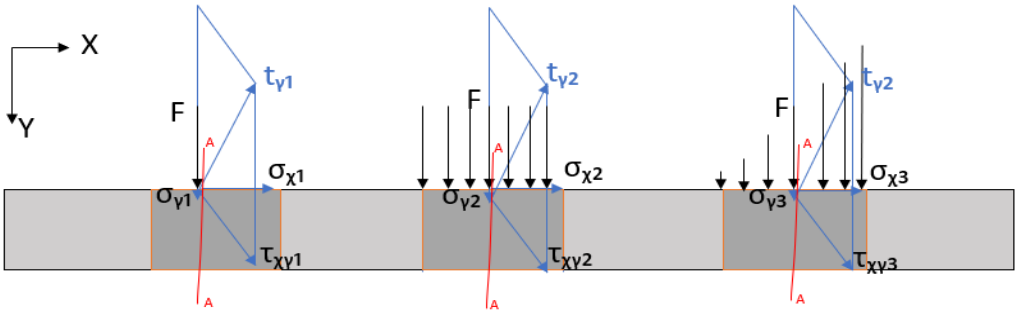

Figure 2. 7 For one point loading, uniform distributed loading, and triangle distributed loading &infinite medium model that is subjected to various types of loading, shear and stress forces

By analyzing this stress distribution on the A-A section in the Figure 2.7, we can obtain a deeper understanding of how the cell will react to different types and levels of pressure. This knowledge is crucial for optimizing the design and placement of the cells, ultimately maximizing their potential for energy generation.
For elastic material [27] we can write:

$$\sigma = e.\epsilon \tag{2.10}$$

According to coordinator system (X, Y) we can write the equation (2.10) as follow:

$$\begin{bmatrix} \sigma_1 \\ \sigma_2 \\ \tau_{xy} \end{bmatrix} = \begin{bmatrix} c_{11} & c_{12} & 0 \\ c_{12} & c_{22} & 0 \\ 0 & 0 & c_{33} \end{bmatrix} \begin{bmatrix} \epsilon_1 \\ \epsilon_2 \\ \gamma_{12} \end{bmatrix} \tag{2.11}$$

As calculating the stiffness matrix, we must be knowing Young's Moduli (e`=22.4 GPa), Poisson's Ratios (υ=0.33) and Shear Moduli (G= 22.4 GPa) also the compliance matrix (S) equal to inverse of stiffness matrix(c) so that we can find the:

$$S_{11} = S_{22} = \frac{1}{e`} \quad , \quad S_{12} = S_{21} = \frac{\upsilon}{e`} \quad , S_{33} = \frac{1}{G} \quad , \quad \epsilon_1 = \frac{\partial x}{\partial X} , \quad \epsilon_2 = \frac{\partial y}{\partial Y} , \quad \gamma_{12} = \frac{\partial x}{\partial Y} + \frac{\partial y}{\partial X}$$

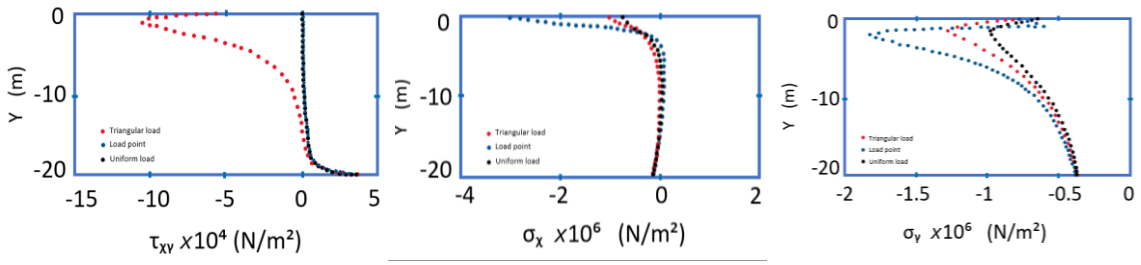

Figure 2. 8 visual representation of the stress distribution σ_x, σ_y, and τ_{xy}, in the piezoelectric cell along A-A section under three loads of point, triangular, and uniform

Under point load conditions, the maximum normal stress (σ_y) is approximately 1.78 × 10⁶ N/m², while the minimum normal stress (σ_y) is around 0.96 × 10⁶ N/m² under uniform distribution load conditions. For normal stress (σ_x), the maximum stress under point load conditions is found to be 0.12 × 10⁶ N/m², with the stress distribution under uniform and triangular loads appearing relatively close together. Regarding shear stress (τ_{xy}), the maximum stress is observed under triangular load conditions, with a value of approximately 10.3 × 10⁴ N/m². The piezoelectric material was found to generate 76.7 Volts.

2.2.2 Piezoelectric with magneto strictive materials (second case)

In this design it is possible to use two mechanisms simultaneously as:
1). By using the magnetostrictive effect of Fe-Si-B-C, stray magnetic fields (H) can stimulate longitudinal strain through the magnetoelectric effect then give electricity (magnetoelastoelectric) [28].
2). By piezoelectric effect causes strain through mechanical vibrations and generate electricity.

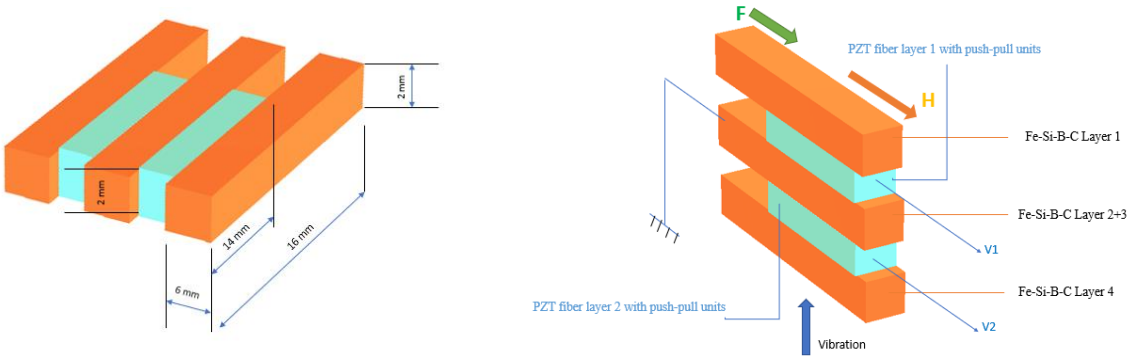

Figure 2.9 Schematic Illustration of energy harvesting for second case

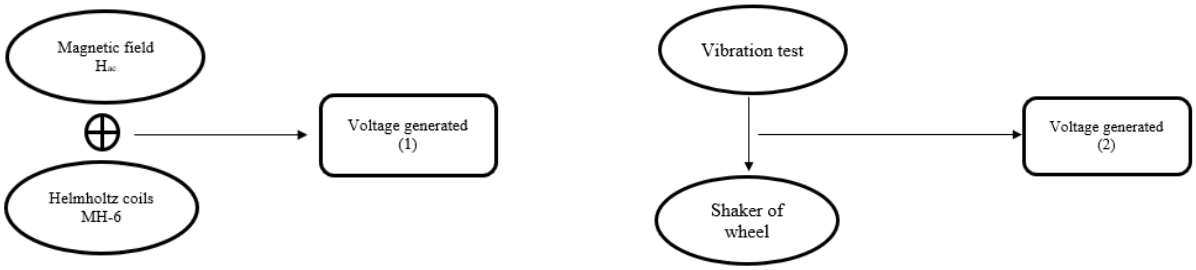

a *b*

Figure 2.10 Schematic diagram of the a. first generation & b. second voltage generation

The relationship between induced voltage (V) and power (P) resulting from an applied magnetic field (H)[29]. The power output (P) can be calculated by the formula:

$$P = V^2/R' \quad (2.12)$$

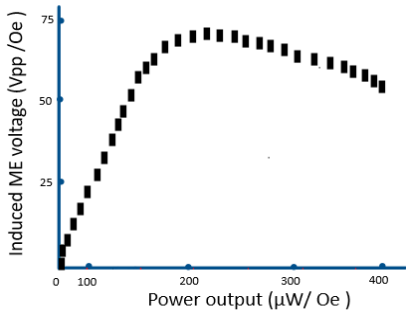

Figure 2.11 Relation between power and voltage for First generation

During vibration testing, mechanical excitation was applied to the magnetoelectric (ME) laminates using shakers equipped with wheels. The response of the laminates to these excitations was monitored using a PCB Piezotronics accelerometer (Model U352C22 with

meter 482A16), specifically calibrated for accurate vibration measurement.The testing procedure leveraged the piezoelectric effect, wherein mechanical deformation of the ME laminates induced an electrical potential. This phenomenon arises from internal charge separation within the piezoelectric material as a result of applied stress. Voltage signals generated from these deformations were recorded for both layers of the laminate: V_1 (first layer) and V_2 (second layer), as shown in Figure 2.12

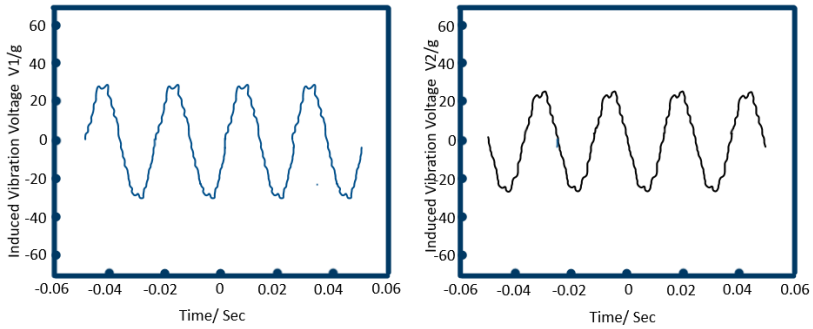

Figure 2.12 Induced voltage generate per first layer V1 and second layer V2

2.3 ROADS (INFRASTRUCTURE) EFFECTS FOR OTHER HARVESTING ENERGY

Electric Roads as a Core Component of the Harvesting Charging Station (HCS), which enable continuous energy harvesting from rotating vehicle tires. These studies highlight the potential of different energy harvesting techniques, such as piezoelectric, triboelectric, and magnetic, to contribute to the generation of electricity in innovative ways. By incorporating these technologies into our HCS, we can harness these untapped energy sources and make strides towards a more sustainable and efficient transportation infrastructure[30]. The harvesting charging station is represented as shown in the following

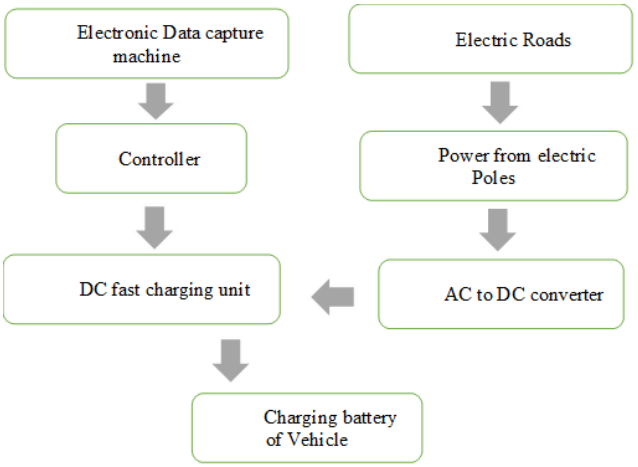

Figure 2. 13 The flowchart of Harvesting Charging Station (HCS)

Design and Construction of Roads Harvesting Energy There are six configurations (LAD1 to LAD6) of road-integrated piezoelectric harvesting systems introduced:

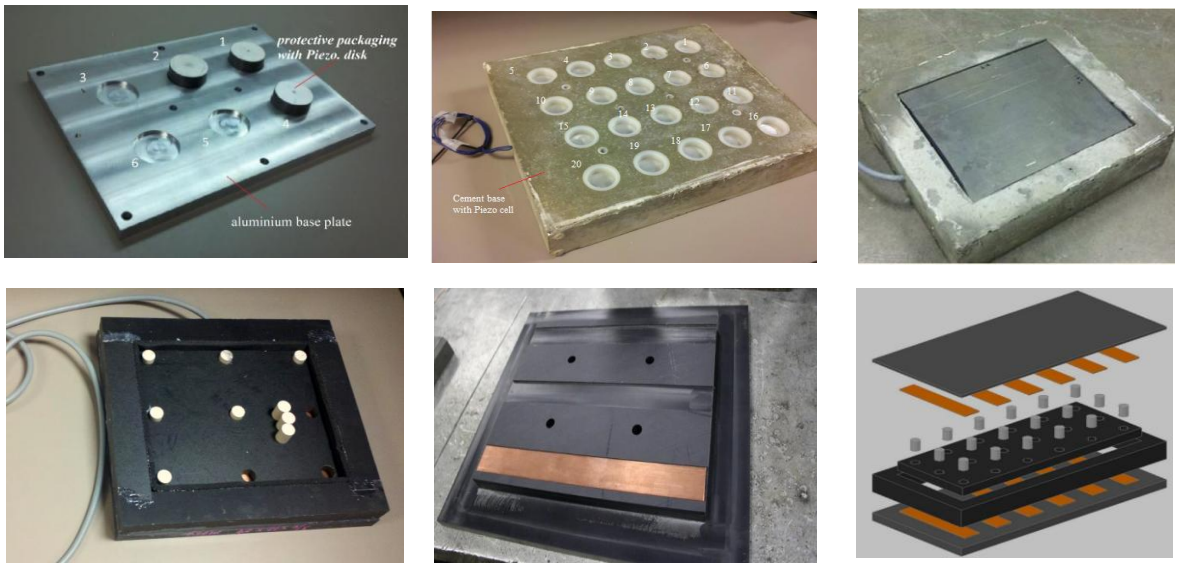

In order to evaluate the performance of LAD1, LAD2 and LAD3, it is crucial to consider LAD1 as it provides insights into the energy production or harvesting capabilities. The testing of LAD1 is conducted using a model mobile loading simulator (MMLS) provided by PAVETESTING company with the device Pave®MMLS11 which it rented. This simulator comprises a small wheel that rotates on top of the piezoelectric layer, as depicted in Figure 2.14. We have obtained three specimens from Zibo Yuhai Electronic Ceramic Co., Ltd. These specimens are categorized as single-layer stacks, double-layer stacks, and four-layer stacks. A schematic of the experimental setup is presented to illustrate the force measurement procedure. Each specimen is placed atop a force meter and connected to a load resistance, with a steel stabilizer positioned between them to ensure stability. The entire setup is integrated with an electric shaker and monitored using Lab Master software, which enables real-time data acquisition via computer interfacing. During testing, various loading resistances are applied, and the resulting voltage output is recorded to assess the specimen's electrical response. Notably, a voltage signal of 1.2 V corresponds to 90.4 N of applied force, serving as the calibration reference for force conversion.

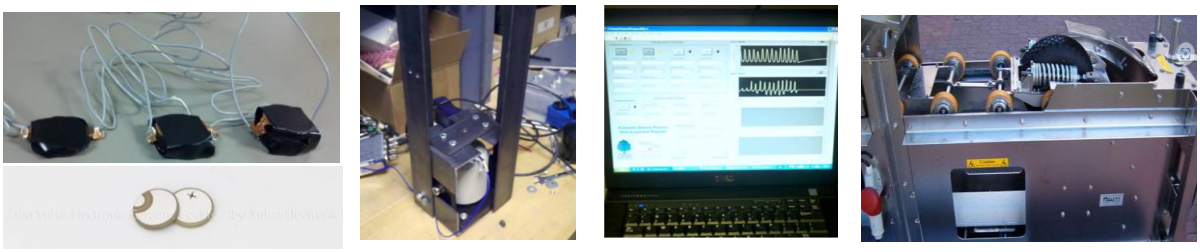

Figure 2. 14 testing LAD1

To calculate the power/force ratio from the output voltage, there is relationship between electrical energy and mechanical work or force and that relationship combines both electrical and mechanical aspects. The equation can be interpreted as:

$$\frac{P}{F} = \frac{\int V^2\, dt}{R \int F\, dt} \tag{2.13}$$

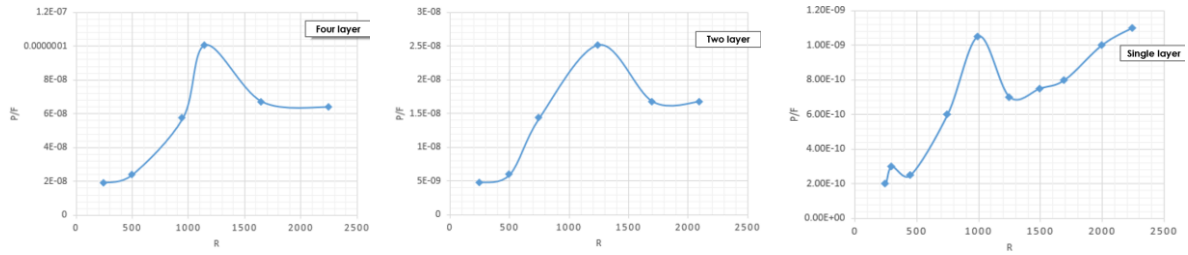

Figure 2. 15 The graph between P/f & R for the one, two and four-layer generator

The testing LAD4 procedure for the piezoelectric cells in the LAD1 design follows a similar approach MMLS, utilizing the same type of PZT-51 discs. With reference to equation 2.13, we can summarize the observations for LAD4 and LAD5 as follows for For 10,20,40,and60 MΩ.

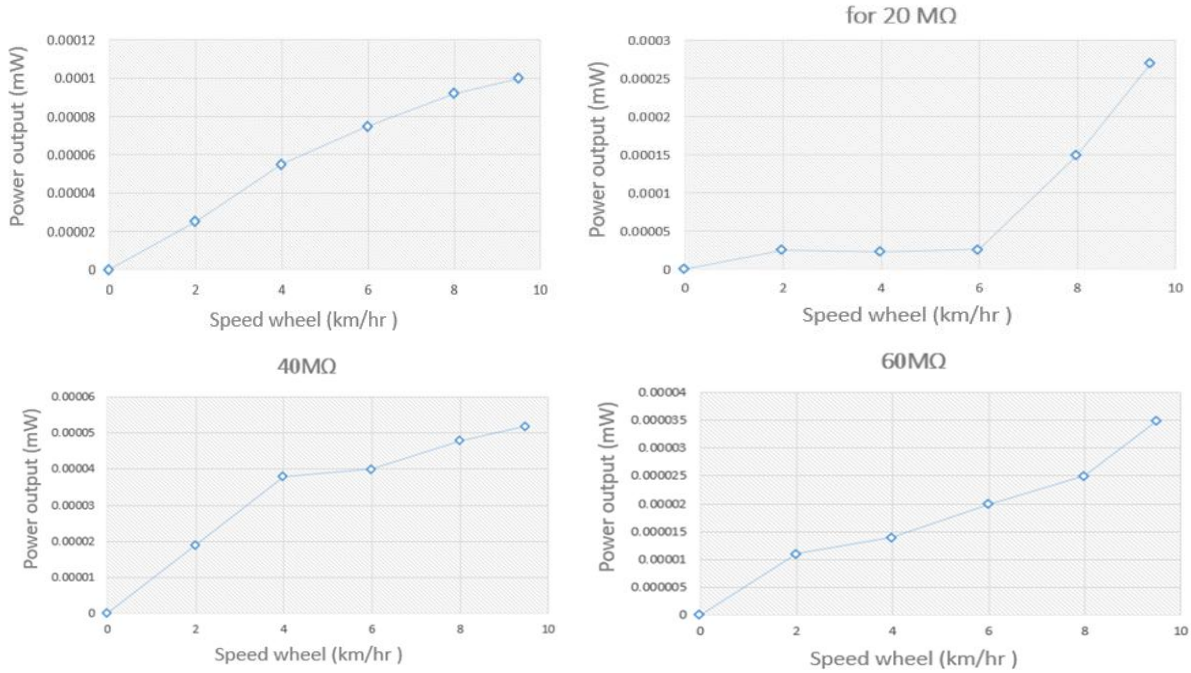

Figure 2. 16 The relation between power and speed wheel with different loading resistance

The voltage output of an Electric Road Energy Harvesting Vehicle (EREHV) system comprising models EREHV1, EREHV2, and EREHV3 is influenced by several factors, including wheel speed, load resistance, and harvester design layout. At a constant speed of 9.5 km/h and a load resistance of 20 MΩ, each harvester model demonstrated distinct voltage responses (see Figure 2.17 for EREHV data). Increasing wheel speed enhances voltage output when resistance is fixed, while increasing resistance reduces output at a constant speed .Design differences across harvester models lead to voltage variation, even under identical test conditions. Voltage waveforms reveal periodic peaks approximately every four seconds, likely corresponding to wheel rotation cycles. Additionally, positive voltages were recorded under loaded wheel conditions, whereas negative voltages occurred during wheel disengagement, indicating that axial load plays a critical role in energy generation performance.

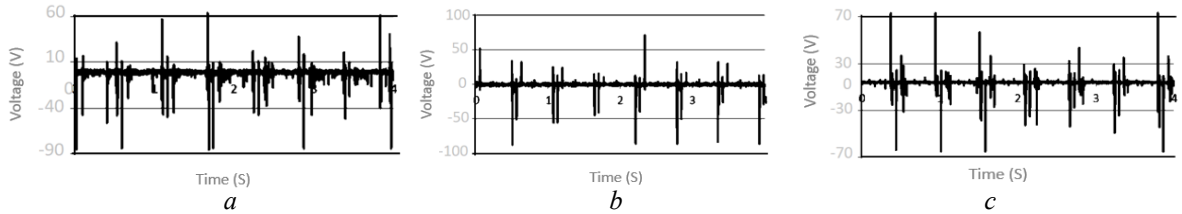

a *b* *c*

Figure 2. 17 The graph of voltage for a. EREHV1, b. EREHV2, c. EREHV3 at 3.2Km/h

2.4 ELECTROMECHANICAL EFFECTS BY MMR FOR OTHER HARVESTING ENERGY

The MMR consists of key mechanical components: pedals, rack & pinion, gearbox, coupling, and a generator.The Pedal Harvesting Energy (PHE) module stores and channels force from foot pressure into mechanical work.

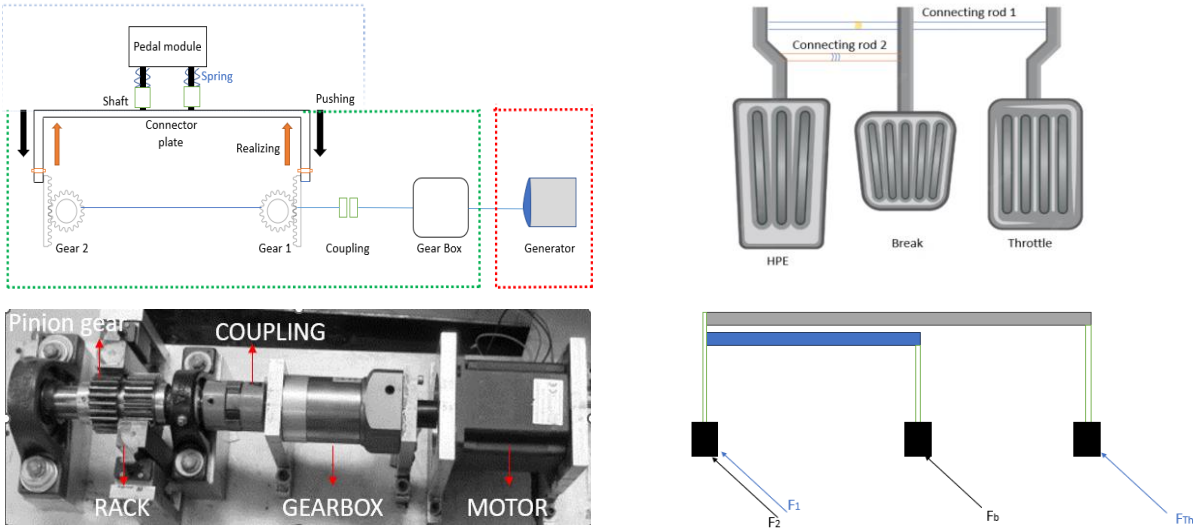

To find the equation for the above circumstance involving the MMR, it is necessary to sketch the torques and inertia associated with the system. To begin, a sketch of the MMR should be created, clearly identifying the places of the angular displacement and axis of rotation, as shown in Figure 2.18, According to Newton's second law of motion, we can express the equation of motion for the Pedal Harvesting Energy (PHE) system as follows:

$$F_t = M_b \,.\ddot{x} + C_b \,.\dot{x} + k_b.x \qquad (2.14)$$

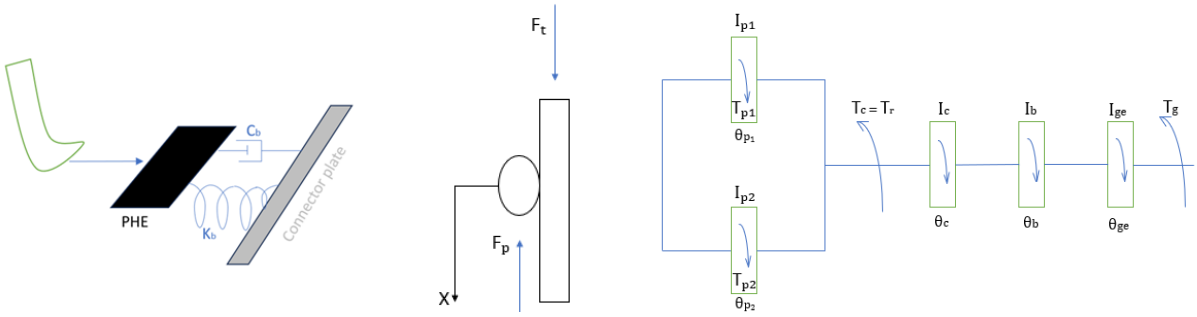

Figure 2. 18 The moment of inertia and torques of MMR

Now write the dynamics equations for rack, pinion and outer ring of one-way clutch, and coupling, gearbox and generator in MMR we can find:

$$\mathrm{M_r}\,.R.\ddot{\theta} + \frac{K}{R}(I_{\mathrm{p,n}} + I\mathrm{ge}\,.\mathrm{n}` + I\mathrm{c}\,)\ddot{\theta} + \frac{K}{R}.\mathrm{K_t}\,.\mathrm{I} = \mathrm{F_t}$$

$$[\mathrm{M_r}\,.R + \frac{K}{R}(I_{\mathrm{p,n}} + I\mathrm{ge}\,.\mathrm{n}` + I\mathrm{c}\,)]\ddot{\theta} + [\frac{K.\mathrm{K_t}\,.K_g.\mathrm{n}`}{R.\mathrm{R_t}}]\dot{\theta} = \mathrm{F_t}$$

$$M_{\mathrm{e}}\,.\ddot{\theta} + \mathrm{C_e}\,.\dot{\theta} = \mathrm{F_t}$$

$$\ddot{\theta} = \frac{1}{M_{\mathrm{e}}}\mathrm{F_t} - \frac{\mathrm{C_e}}{M_{\mathrm{e}}}.\dot{\theta} \qquad (2.15)$$

When a system is disengaged, the mechanical linkage between the driving force and the generator shaft is interrupted. As a result, the generator shaft continues to rotate due to its inertia, but this rotational motion gradually diminishes over time. Therefore, the angular displacement of the generator can be instead ($\dot{\theta}_{ge}$) as follows:

$$\dot{\theta}\mathrm{ge} = \dot{\theta}\mathrm{ge}\,.e^{-\alpha t} \qquad (2.16)$$

Based on equations (2.14), (2.15) and (2.16), it has been determined that the harvesting of energy can be achieved. The power can be calculated either from the angular velocity ($\dot{\theta}$) or from the linear velocity ($\dot{x}$) as follows:

$$P = \mathrm{C_e}\,.\dot{\theta}^{2} \qquad (2.17)$$

We can write the equation (2.14) as follows:

$$\ddot{\mathrm{x}} = \frac{1}{\mathrm{Mb}}\mathrm{F_t} - \frac{\mathrm{Cb}}{\mathrm{Mb}}\dot{\mathrm{x}} - \frac{\mathrm{kb}}{\mathrm{Mb}}\mathrm{x} \qquad (2.18)$$

The gain block in Simulink for equation (2.18) comes from the tested indicators which we take in following schedule:

Table 2. 9 Information about the tested indicators for simulation MMR

Name	Notation	Value and unit
Equivalent mass	M_{eq}	207.25 kg
Pressing mass	M_b	50 kg
Equivalent coefficient when Rt =202Ω	C_{eq}	28.65 (N-s/m)
Pinion stiffness	K	0.5024 (N/m)
Generator stiffness	K_t	0.18 (N/m)
PHE stiffness	K_b	1300 (N/m)
PHE coefficient	C_b	700 (N-s/m)

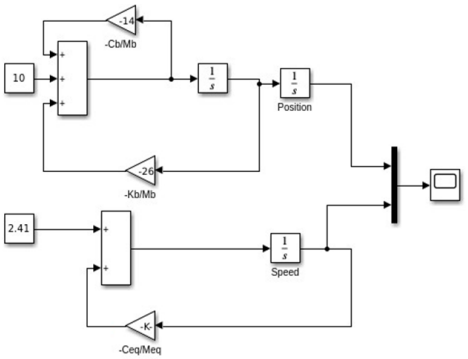

Since (Ft) is related through (M_b) between the brake pedal and the throttle pedal :

$$F_{\mathrm{t}} = M_b\,.\mathrm{g} \qquad (2.19)$$

Table 2.10 Information about pressing mass for small and big cars

Type	Small or family car	Big car
Brake pedal	(23- 45) kg	(45-68) kg
Throttle pedal	(9-23) kg	(23-45) Kg

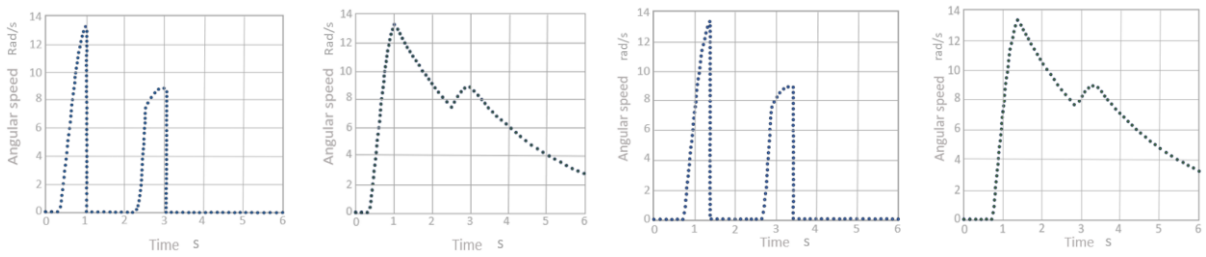

a *b*

Figure 2.19 The angular speed of generator & pinion plots to time for a: for 8.04 KMH of car speed and b: 3.21KMH of car speed

In order to study the impact of external loads on energy production, it is crucial to incorporate simulations. Testing different resistances connected to the generator provides valuable insights into current behavior and aids in determining the energy harvested through this method. The simulation was conducted within a speed range of 11.26 - 16.09 km/h. Figure 2.20 illustrates the results, showcasing two pressure peaks at PHE that generate power. For a resistance value of 110 Ω, the first peak yielded approximately 1145 watts, while the second peak produced around 735 watts. These studies provide valuable information regarding the output harvesting energy under varying load conditions.

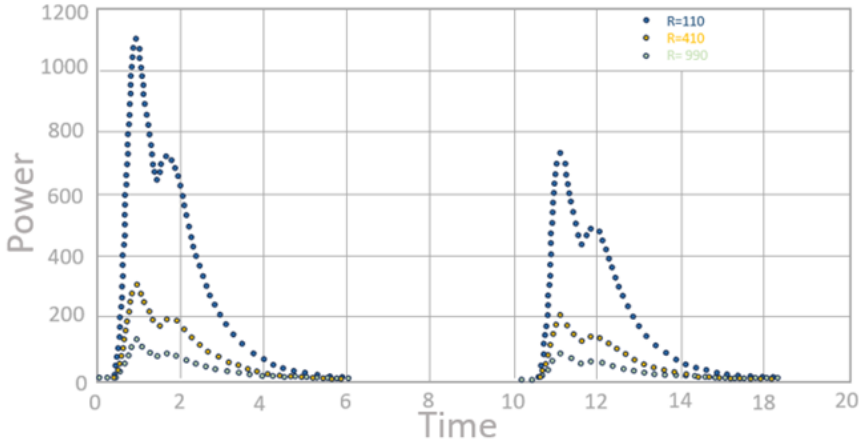

Figure 2.20 The generating power with time and different resistance

3 NEW SCIENTIFIC RESULTS – THESES

T1. The harvesting energy by electromagnetic effects as Radial & Axial Design (RD & AD):

In this study, I propose a novel method for energy production and harvesting from wheel movement, distinct from traditional approaches that focus on vibrations or suspensions. This strategy aims to assist hybrid or electric vehicles in charging their batteries while in motion, without the need to stop. The process involves converting the rotational motion of the wheels into electrical energy through electromagnetic principles, a concept that has been explored by various researchers.This research demonstrates that energy can be harvested from the rotation of the wheels on first case as RD design, approximately 2.5 mW of energy is generated by capturing the motion of magnets through the wheel's movement within a coil, in accordance with Faraday's law. This process was simulated using MATLAB, yielding a 2% error based on the magnetic dipole value. For another AD design, this energy harvester produced about 4.02 mW of power, also with a 3% error between the experimental data and the model at 53 rpm. (1)(5)

T2. The harvesting energy by Piezoelectric materials inside the wheel:

In my study, I focused on the piezoelectric material PZT-5J because of its excellent mechanical strength and durability. I conducted a detailed analysis of the stress distribution within this material, aiming to optimize the performance of a piezoelectric energy harvester integrated into a vehicle damper system. To evaluate its effectiveness, I examined two different energy harvesting scenarios under varying mechanical conditions. In the first scenario, utilizing the specified materials, approximately 600 μW was generated at a pressure of 0.71×10^6 N/m² over an area of 0.01716 m². Conversely, with a piezoelectric cell area of 40 m² and a charge density of about 0.34 A, the output surged to 26 W. In the second scenario, the combination of piezoelectric and magnetostrictive effects resulted in an energy harvest of approximately 826 μW. Within the field of piezoelectric applications, there is a pressing need to improve power output by investigating various designs. The efficiency of piezoelectric materials tends to decline over time, specifically between 1 to 5 minutes, with efficiencies ranging from 13.4% to 14.5%. To counteract this issue, it could be advantageous to implement multiple layers of these materials—potentially doubling or tripling them—within the wheel and conducting a comprehensive performance study. (4)(6)(9)

T3. The harvesting energy by the piezoelectric roads:

My research supports the concept of a smart city by utilizing PZT materials with several assembly designs integrated into road layouts (LAD1, LAD2, LAD3, LAD4, LAD5, and LAD6). These designs generate energy that is transmitted to electric poles installed along the roads. A converter then transforms the output from AC to DC, enabling this energy to power vehicles and charge car batteries without requiring stops(smart roads) or in any place there is HCS with stop of car. For instance, in the case of LAD1 with a resistance of 335 KΩ, the power output was approximately 3×10^{-5} W. Likewise, with a resistance of 565 KΩ, the output

increased to around 3.5×10^{-4} W. In the case of LAD4 at a speed of 9.5 km/hr, a resistance of 20 MΩ yielded a similar power output of 0.275 mW. (3)(7)(8)(11)

T4. The harvesting energy by MMR:

This research introduces an innovative approach to energy harvesting from car pedals, distinguishing it from prior studies that predominantly focused on bike pedal . While previous investigations have explored energy harvesting from pedals in the context of Formula racing cars using manual methods, our research pioneers a new domain by emphasizing the potential of car pedals for energy generation. This study demonstrates that the energy which produce is coming from MMR that achieves the conversion of linear motion from racks into rotational motion by interlocking pinion gears 1 and 2. When the driver vertically presses the pedal module, the rack moves, causing the pinion gear to rotate and the shaft to spin. This rotation of the shaft drives the gearbox, which in turn rotates the DC motor, generating electric power. It is equal approximately by simulated with MATLAB about 1100 to 1145 W and when increase the pressing of both of the pedals will be increase the output of energy also the number of pressings on pedals. In the context of MMR, conducting a stress analysis on critical components such as the connecting rod, foot cover, and rack and pinion gear assembly would be valuable. Investigating their failure modes can provide insights that future researchers can use to enhance the overall efficiency of the device. Additionally, comprehensive and rigorous in-field testing is essential to analyze the actual impact of the driver's leg on the pedals, particularly by leveraging the brake pedal during periods of heavy vehicle congestion, as well as to examine vehicle dynamics more thoroughly. (2)(10)

4 LIST OF PUBLICATIONS RELATED TO THE TOPIC OF THE RESEARCH FIELD

(1) Mohammed Alaa Alwafaie, Bela Kovacs: empowering sustainability: The promise of energy harvesting from wheel motion (experiment and simulation). International Journal of Membrane Science and Technology, VoL.10 No. (4), pp 1517-1524, 2023 https://doi.org/10.15379/ijmst.v10i4.2271, MTMT No. 34550348, Rank: Q4.

(2) Mohammed Alaa Alwafaie, Bela Kovacs: the mechanism parts of mechanical motion rectifier to produce energy from third pedal in automotive, Acta Tecnología - International Scientific Journal about Technologies, Volume: 9,2023 Issue: 2 Pages: 73-77, ISSN 2453-675X, Article DOI: https://doi.org/10.22306/atec.v9i2.174, MTMT NO. 34133445.

(3) Mohammed Alaa Alwafaie, Bela Kovacs: testing LAD1of harvesting electric roads, Acta Mechatronica -International Scientific Journal about Mechatronics, Volume: 7 2022 Issue: 4 Pages: 25-29 ISSN 2453-7306, MTMT NO.33662173, Article: doi:10.22306/am. v7i4.87.

(4) Mohammed Alaa Alwafaie, Bela Kovacs: dual - harvester energy (type3), Open Access Research Journal of Science and Technology,2022,04(02),067-071, MTMT NO.32769437, Article DOI: https://doi.org/10.53022/oarjst.2022.4.2.0037.

(5) Mohammed Alaa Alwafaie, Béla Kovács: harvester wheel energy (type1), Quest Journals: Journal of Research in Mechanical Engineering, Volume 8 ~ Issue 1 (2022) pp:06-11ISSN(Online)2321-8185,2022, MTMT NO. 32653475, http://www.questjournals.org/jrme/papers/vol8-issue1/B08010611.pdf

(6) Mohammed Alaa Alwafaie, Béla Kovács: harvester wheel energy (type 4), World Journal of Advanced Research and Reviews, 2022, 13(02), 304–308, MTMT 32695809, Article DOI: https://doi.org/10.30574/wjarr.2022.13.2.0147

(7) Mohammed Alaa Alwafaie, Béla Kovács: electric charging platforms, International AEGEAN conferences on Innovation Technologies and Engineering V AEGEAN, February 25-26, 2022 / Izmir, Turkey, pp 33-37 (2022), MTMT no: 32769342.

(8) Mohammed Alaa Alwafaie, Bela Kovacs: the review of infrastructure requirements for electric automotive, in 6. International Ankara multidisciplinary studies congress, October 13-14, 2023, Ankara, Turkey. 74-77. MTMT No. 34550378.

(9) Mohammed Alaa Alwafaie, Bela Kovacs: studying the distribution of stress in two-dimensional compression piezoelectric cells under load-truck conditions, in 61st International Scientific Conference on experimental stress analysis 2023, June 6th – 8 th, 2023, Košice, Slovakia. 117-124, MTMT NO. 34788590 (Scopus index).

(10) Mohammed Alaa Alwafaie, Bela Kovacs: Investigating the feasibility of energy harvesting from the third pedal in automotive systems using a mechanical motion rectifier: simulation-based study, Acta Tecnología - International Scientific Journal about Technologies, Volume: 10 2024 Issue: 2 Pages: 57-64 ISSN 2453-675X, Article DOI: https://doi.org/10.22306/atec.v10i2.200

(11) Mohammed Alaa Alwafaie, Bela Kovacs: Design and evaluation of test assembly (LAD5) for electric road energy harvesting (EREH), AIP Conf. Proc. 3227, 030001 (2025), Volume 3227, Issue 1, 12 March 2025, https://doi.org/10.1063/5.0241749

5 REFERENCES

[1] International Journal for Scientific Research and Development (IJSRD). (2016). Study of energy recovery systems in automobile industry. https://ijsrd.com/articles/IJSRDV4I30396.pdf

[2] Ehsani, M., Gao, Y., Longo, S., & Ebrahimi, K. (2018). Modern electric, hybrid electric, and fuel cell vehicles. CRC press.

[3] Fédération Internationale de l'Automobile (FIA). (2023). Formula One technical regulations: Energy recovery systems. https://www.fia.com/regulation/category/110

[4] Honda Motor Co. (2022). *Evolution of hybrid technologies (MGU-H, MGU-K) – 2015 to 2022*. https://global.honda/en/tech/motorsports/Formula-1/Powertrain_MGU-H_MGU-K/

[5] Li, M., Lu, J., Chen, Z., & Amine, K. (2018). Automotive Li-ion batteries: Status and future perspectives. Automotive Innovation, 1(1), 4–13. https://doi.org/10.1007/s41918-018-0022-z

[6] Cai, W., Wu, X., Zhou, M., Liang, Y., & Wang, Y. (2021). Review and development of electric motor systems and electric powertrains for new energy vehicles. Automotive Innovation, 4(1), 3–22. https://doi.org/10.1007/s42154-021-00139-z

[7] Rubio, J., Zacarias, A., Pacheco, J. (2025). Dynamic Model of an Electric Vehicle with Energy Recovery. In: Dynamic Models of Energy, Robotic, and Biological Systems. Springer, Cham. https://doi.org/10.1007/978-3-031-85438-5_3

[8] IEEE. (n.d.). Kinetic Energy Recovery Systems for Racing Cars. IEEE Xplore. https://ieeexplore.ieee.org/book/8505026

[9] Smith, J., & Lee, A. (2023). Advanced energy recovery systems in Formula One: MGU-K and MGU-H integration. IEEE Transactions on Vehicular Technology, 72(4), 1234–1245. https://doi.org/10.1109/TVT.2023.1234567

[10] Koundal, S., Sharma, S. L., & Debbarma, A. (2025). Battery thermal management systems for electric vehicles: An overview of cooling techniques and performance optimization. Journal of Thermal Analysis and Calorimetry. https://doi.org/10.1007/s10973-025-14170-3

[11] Zhang, Y., & Wang, C. (2018). A battery-supercapacitor hybrid energy storage system design and control strategy. International Journal of Pure and Applied Mathematics, 119(15), 277–284. https://www.acadpubl.eu/hub/2018-119-15/2/277.pdf

[12] Li, X., & Palazzolo, A. (2022). A review of flywheel energy storage systems: State of the art and opportunities. Journal of Energy Storage, 46, 103576. https://vcef.engr.tamu.edu/wp-content/uploads/sites/231/2023/08/A-review-of-flywheel-energy-storage-systems-state-of-the-art-and-opportunities.pdf

[13] Alghamdi, A., & Mohammed, O. A. (2024). Energy storage systems: Technologies and high-power applications. Batteries, 10(4), 141. https://doi.org/10.3390/batteries10040141.

[14] Miller, J. M., & Burke, A. F. (2010). Power electronics in hybrid vehicles. IEEE Transactions on Power Electronics, 25(3), 585–592. https://doi.org/10.1109/TPEL.2009.2039353

[15] Aksu, U., & Halicioglu, R. (2018). A review study on energy harvesting systems for vehicles. Tehnički glasnik, 12(4), 251-259.

[16] Sultoni, A. I., Sutantra, I. N., & Pramono, A. S. (2013). Vibration energy harvesting on vehicle suspension using rotary and linear electromagnetic generator. IPTEK The Journal for Technology and Science, 24(1), 1.

[17] Wang, Y. J., Shen, S. C., & Chen, C. D. (2012). Wideband electromagnetic energy harvesting from a rotating wheel. Small-Scale Energy Harvesting, 10.

[18] Zhou, M., Wang, L., Wang, J., Ding, G., & Liu, Z. (2023). Research progress and latest achievements of road piezoelectric vibration energy capture technology based on intelligent transportation construction. Intelligent Transportation Infrastructure, 2, liad014.

[19] Lazaroiu, G. C., & Roscia, M. (2012). Definition methodology for the smart cities model. Energy, 47(1), 326-332.

[20] Wang, Z., He, L., Gu, X., Yang, S., Wang, S., Wang, P., & Cheng, G. (2021). Rotational energy harvesting systems using piezoelectric materials: A review. Review of Scientific Instruments, 92(4).

[21] Wu, C., Wang, A. C., Ding, W., Guo, H., & Wang, Z. L. (2019). Triboelectric nanogenerator: a foundation of the energy for the new era. Advanced Energy Materials, 9(1), 1802906.

[22] Faraday, M. (1831). Experimental researches in electricity. Philosophical Transactions of the Royal Society of London, 122, 125–162. https://doi.org/10.1098/rstl.1831.0007

[23] Westfall, R. S. (1980). Never at rest: A biography of Isaac Newton. Cambridge University Press.

[24] Alwafaie, M. A. ., & Kovacs, B. . (2023). Empowering Sustainability: The Promise of Energy Harvesting from Wheel Motion (Experiment and simulation). International Journal of Membrane Science and Technology, 10(4), 1517-1524. https://doi.org/10.15379/ijmst.v10i4.2271

[25] Wu, J. (2018). BaTiO3-Based Piezoelectric Materials. In: Advances in Lead-Free Piezoelectric Materials. Springer, Singapore. https://doi.org/10.1007/978-981-10-8998-5_5

[26] Panda, P.K., Sahoo, B., Thejas, T.S. et al. High d33 Lead-Free Piezoceramics: A Review. J. Electron. Mater. 51, 938–952 (2022). https://doi.org/10.1007/s11664-021-09346-0

[27] Timoshenko, S. P., & Goodier, J. N. (1970). Theory of elasticity (3rd ed.). McGraw-Hill. [Classic reference for elasticity theory].

[28] Swain, A. B., Dinesh Kumar, S., Subramanian, V., & Murugavel, P. (2020). Engineering resonance modes for enhanced magnetoelectric coupling in bilayer laminate composites for energy harvesting applications. Physical Review Applied, 13(2), 024026.

[29] Nakamura, T., & Ogama, Y. (2024). Relationship between the induced voltage of a rotor bar and the rotation characteristics of a high-temperature superconducting induction motor. Journal of Applied Physics, 136(9).

[30] Khasawneh, M.A. Energy harvesting devices in pavement structures. Innov. Infrastruct. Solut. 10, 183 (2025). https://doi.org/10.1007/s41062-025-01996-x